

# Causal-ICM: A Data Fusion Framework For Heterogeneous Treatment Effect Estimation With Multi-Task Gaussian Processes

**Evangelos Dimitriou**

EVANGELOS.DIMITRIOU.22@UCL.AC.UK

*Department of Statistical Science, University College London*

**Edwin Fong**

CHEFONG@HKU.COM

*Department of Statistics and Actuarial Science, University of Hong Kong*

**Jens Magelund Tarp**

JQMT@NOVONORDISK.COM

*Novo Nordisk A/S*

**Karla Diaz-Ordaz**

KARLA.DIAZ-ORDAZ@UCL.AC.UK

*Department of Statistical Science, University College London*

**Brieuc Lehmann**

B.LEHMANN@UCL.AC.UK

*Department of Statistical Science, University College London*

## Abstract

Bridging the gap between internal and external validity is crucial for heterogeneous treatment effect estimation. [Randomised controlled trials \(RCTs\)](#), favoured for their internal validity due to randomisation, often encounter challenges in generalising findings due to strict eligibility criteria. Observational studies, on the other hand, may provide stronger external validity through larger and more representative samples but can suffer from compromised internal validity due to unmeasured confounding. Motivated by these complementary characteristics, we propose a novel Bayesian nonparametric approach, *Causal-ICM*, leveraging multi-task Gaussian processes to integrate data from both [RCTs](#) and observational studies. In particular, we introduce a parameter that controls the degree of borrowing between the datasets and prevents the observational dataset from dominating the estimation. We propose a data-adaptive procedure for choosing the optimal value of the parameter. *Causal-ICM* outperforms other data fusion methods in point estimation across the covariate support of the observational study and provides principled uncertainty quantification for the estimated treatment effects. We demonstrate the robust performance of *Causal-ICM* in diverse scenarios through multiple simulation studies and a real-world study.

**Keywords:** Data Fusion, Bayesian Nonparametrics, Multitask Gaussian Processes, Generalisability, Heterogeneous Treatment Effects

## 1. Introduction

Treatment effect estimation is an important task in many applications, including medicine, epidemiology, and the social sciences. The goal is to quantify the expected impact of a particular intervention in a given target population. The effect of an intervention within a population may vary systematically with respect to a particular set of covariates. Understanding such treatment effect heterogeneity is critical to ensure that appropriate decisions are taken for all individuals, not just those similar to the average ([Brantner et al., 2023](#)). An appropriate characterisation of the uncertainty of treatment effect estimates is also required to support robust and reliable decision-making. Uncertainty quantification for heterogeneous

treatment effects is challenging, however, especially when making inferences about individuals not represented in the study. Classical methods typically rely heavily on extrapolation without adequate variance inflation outside the study support (Degtiar and Rose, 2023).

The gold standard for treatment effect estimation remains the RCT. The random treatment allocation in the study guards against the effect of confounding. As a result, under standard identifiability assumptions, we can obtain an unbiased estimate of the treatment effect. There are, however, drawbacks to the use of RCTs (Frieden, 2017), such as the high financial cost or the limited sample sizes. While they may be powered enough to detect the Average Treatment Effect (ATE), they are typically underpowered for subgroup effects. Furthermore, strict eligibility criteria and selection bias may lead to a sample non-representative of the target population (National Academies of Sciences, Engineering, and Medicine, 2022). Observational studies provide an alternative source of data for treatment effect estimation. In contrast to RCTs, they generally benefit from larger sample sizes and tend to be more representative of the target population. However, observational studies may suffer from unobserved confounding, i.e. unobserved variables that affect both the outcome of interest and the treatment allocation, and can lead to biased treatment effect estimates. For example, a patient’s underlying health status might influence both the treatment they receive and their eventual outcome, yet remain unmeasured.

The complementary nature of RCT and observational data indicates the potential benefits from combining the two sources to obtain better heterogeneous treatment effect estimates. Such data fusion approaches have received increased interest in recent years. A range of methods have been developed to integrate information from multiple sources of data, including a limited number targeting causal inference problems (Colnet et al. (2023), Lin et al. (2025b)). These typically rely on strong, untestable assumptions about the structure of the confounding effect and, moreover, are often not able to provide uncertainty quantification around the point estimates of heterogeneous treatment effects.

In this paper, we introduce a Bayesian nonparametric approach to obtain both point and uncertainty estimates of heterogeneous treatment effects for the target population. Our approach is based on a multi-output Gaussian process (GP), a natural choice in the data fusion context as it enables joint modelling of the RCT and observational outcome regression functions, and uses the Bayesian machinery to share information and quantify uncertainty of the functions in regions of differing covariate support. Our key contributions are as follows:

- We propose *Causal-ICM*, a multi-task GP model for heterogeneous treatment effect estimation that accurately captures complex functional relationships in the presence of unobserved confounding both within the support of the RCT covariate distribution and when extrapolating beyond it.
- *Causal-ICM* provides principled uncertainty quantification across the full support of the target population. Crucially, we theoretically show that *Causal-ICM* limits the amount of information learnt from the observational dataset, and safeguards against overconfidence in the presence of bias.
- Through a comprehensive set of simulation studies and an application to a real-world dataset, we demonstrate that *Causal-ICM* achieves similar or superior performance both in point estimation and uncertainty quantification relative to a broad set of state-of-the-art causal data fusion methods.

## 2. Related Literature

Heterogeneous treatment effect (HTE) estimation has received renewed interest in recent years. The most common strategy is to focus on the conditional average treatment effect (CATE) function, which quantifies the expected treatment effect given particular covariate values. Under suitable identifiability assumptions (Dahabreh and Hernán, 2019), the CATE can be estimated parametrically - e.g. using linear regression - or non-parametrically, e.g. using nearest-neighbour matching, kernel methods (Brantner et al., 2023), or tree-based methods including causal random forests (Wager and Athey, 2018) and their Bayesian counterpart (Hahn et al., 2020).

Data fusion across an RCT and an observational study has tended to focus on ATE estimation (see Lin et al. (2024) and Colnet et al. (2023) for comprehensive reviews). These methods aim to improve efficiency by integrating information from both sources. Demirel et al. (2024) focus instead on data fusion for generalisability, proposing a framework that builds an observational predictor and then treat the difference between the trial outcome function and that observational predictor as a bias function that captures both confounding and transportation bias due to the differences between the trial and target populations. Similar approaches, although outside the immediate scope of our work, have focused on data fusion for the estimation of long term effects, where randomised data are unconfounded but contain only short term effects, while observational data, although confounded, contain information about long term outcomes (Ghassami et al. (2025), Imbens et al. (2024)).

Data fusion methods for CATE estimation, the focus of this paper, follow three broad lines of work. One strategy is to use experimental data to debias observational estimates by learning a correction or bias function. Kallus et al. (2018) introduce a two-step approach that corrects hidden confounding in the absence of covariate overlap, relying on the strong assumption of linear confounding and the ability to identify this correction term parametrically. Yang et al. (2022b) relax this linearity assumption and provide identifiability and efficiency results under more flexible structural models. Hatt et al. (2022) develop a representation-learning strategy that learns shared features and confounded outcome models from observational data, using the RCT to estimate a bias function that debiases these models, with finite-sample bounds that highlight how performance depends on sample size, distribution shift, and bias complexity. Wu and Yang (2022) propose an R-learner that achieves consistency and asymptotic efficiency under covariate overlap between the RCT and the observational study. A second direction consists of “test-then-pool” strategies, in which the trial and observational datasets are combined only if the observational study appears sufficiently unbiased. For instance, Yang et al. (2023) implement such a strategy, although their approach is limited to linear treatment effect models and relies on strong parametric assumptions. A third line of work uses Bayesian dynamic borrowing to regulate how much information is extracted from the observational study. For instance, Lin and Evans (2023) propose a Bayesian dynamic borrowing approach through a power likelihood to reduce the effect of confounding and control the degree of information we borrow from the observational study.

Our method, *Causal-ICM*, takes a Bayesian dynamic borrowing approach based on multi-task GPs, whereby each potential outcome is treated as a distinct task. Multi-task GPs have been successfully employed for causal inference using solely observational data (Alaa and van der Schaar, 2017) and extended to handle hierarchical hidden confounders

(Witty et al., 2020). Others have built on this framework to develop a general class of counterfactual multi-task deep kernel models that efficiently estimate causal effects and learn policies by stacking coregionalized GPs and deep kernels (Caron et al., 2022). GPs have also been employed as a matching tool for causal inference (Huang et al., 2023). However, these methods are limited to purely observational settings; here we extend these ideas by enabling inference in a data-fusion setting. Our approach is most similar to concurrent work employing multi-task GPs for pseudo-outcome regression to obtain error bounds on the observational bias term (Fawkes et al., 2025).

### 3. Methodology

We begin with a brief introduction on data fusion for HTE estimation. We then introduce a multi-task GPs framework tailored for this purpose. Throughout the paper, we use bold-face to denote vectors, e.g.  $\mathbf{x}$ , and capitals to denote matrices, e.g.  $X$ .

#### 3.1. Data Fusion for Heterogenous Treatment Effect Estimation

In this work, we focus on combining information from an observational dataset and a RCT (experimental) dataset. We begin with some notation. Let  $S \in \{o, e\}$  indicate the study, with ‘e’ denoting the experimental sample and ‘o’ the observational one. Let  $A \in \{0, 1\}$  be the binary treatment indicator. We observe the same baseline covariates in both studies, so each individual has  $\mathbf{X} \in \mathcal{X}^S \subseteq \mathbb{R}^p$ , where  $\mathcal{X}^e$  and  $\mathcal{X}^o$  overlap but  $\mathcal{X}^o$  is not necessarily contained in  $\mathcal{X}^e$ . Without loss of generality we divide the baseline covariates into three subsets, the treatment effect modifiers,  $\mathbf{X}_\tau \in \mathcal{X}_\tau^e$ , the confounders,  $\mathbf{X}_W \in \mathcal{X}_W^e$ , and the selection variables,  $\mathbf{X}_S \in \mathcal{X}_S^e$ , such that  $\mathbf{X} = \mathbf{X}_\tau \cup \mathbf{X}_W \cup \mathbf{X}_S$ . Finally, we observe a continuous outcome  $Y \in \mathbb{R}$ . The counterfactual outcome  $Y_i^a$  denotes the value individual  $i$  would have had under treatment  $A = a$ . The causal estimand of interest is the CATE comparing  $A = 1$  versus  $A = 0$  in the target population given the baseline covariates  $X$ , defined as

$$\tau(\mathbf{x}_\tau) = \mathbb{E} [Y^{a=1} - Y^{a=0} | \mathbf{X}_\tau = \mathbf{x}_\tau]$$

for  $\mathbf{x}_\tau \in \mathcal{X}^e \cup \mathcal{X}^o$ . The difference in the conditional expectations of the outcomes in each study is

$$\omega^s(\mathbf{x}_\tau) = \mathbb{E} [Y | \mathbf{X}_\tau = \mathbf{x}_\tau, A = 1, S = s] - \mathbb{E} [Y | \mathbf{X}_\tau = \mathbf{x}_\tau, A = 0, S = s].$$

The fundamental problem of causal inference is that for each unit we cannot observe both potential outcomes simultaneously. Hence, we make the following identifiability assumptions, which are standard in the literature (e.g. Lanners et al. (2025), Shi et al. (2023)):

A1 Consistency:  $A = a \Rightarrow Y = Y^a$

A2 Mean conditional exchangeability over treatment for the treatment contrast given  $\mathbf{X}_\tau$  in the RCT

$$\mathbb{E}[Y^1 - Y^0 | \mathbf{X}_\tau, S = e] = \mathbb{E}[Y^1 | A = 1, \mathbf{X}_\tau, S = e] - \mathbb{E}[Y^0 | A = 0, \mathbf{X}_\tau, S = e]$$

A3 Positivity of treatment assignment in the RCT:  $P(A = a | \mathbf{X}_S = \mathbf{x}_S, S = e) > 0$  for  $\mathbf{x}_S \in \mathcal{X}_S^e$ .

A4 Mean conditional exchangeability over selection into the **RCT** for the treatment contrast given  $\mathbf{X}_\tau, \mathbf{X}_S$ :

$$\mathbb{E}[Y^1 - Y^0 \mid \mathbf{X}_\tau \cup \mathbf{X}_S] = \mathbb{E}[Y^1 - Y^0 \mid \mathbf{X}_\tau \cup \mathbf{X}_S, S = e]$$

A5 Positivity of **RCT** participation:  $P(S = e \mid \mathbf{X}_S = \mathbf{x}_S) > 0$  for  $\mathbf{x}_S \in \mathcal{X}_S^e$

Under assumptions **A1** - **A5** the **CATE** can be identified from the **RCT** data as

$$\tau(\mathbf{x}_\tau) = \omega^e(\mathbf{x}_\tau)$$

for  $\mathbf{x}_\tau \in \mathcal{X}_\tau^e$ . The derivation is provided in the Appendix **A**. For notational simplicity, and with a slight abuse of notation, we henceforth use  $\mathbf{X}$  and  $\mathbf{x}$  to denote any subset of covariates, whether treatment-effect modifiers or selection covariates.

Conversely, relative to the **RCT**, the covariate distribution of the observational study may be more representative of the target population. In the presence of unmeasured confounding, however, it is not possible to identify  $\tau(\mathbf{x})$  from the observational data alone. In particular, the hidden confounding effect in the observational data, denoted by  $\eta(\mathbf{x}) = \tau(\mathbf{x}) - \omega^o(\mathbf{x})$ , is nonzero. As a result, estimates of  $\omega^o(\mathbf{x})$  may be biased for the estimand  $\tau(\mathbf{x})$ .

In this work, we use a multi-task Gaussian process to jointly estimate  $(\omega^o(\mathbf{x}), \omega^e(\mathbf{x}))$ , treating the two data sources as separate tasks. This leverages both the unbiasedness of the **RCT** and the broader covariate support of the observational study, while adaptively accounting for confounding by comparing  $(\omega^o(\mathbf{x}), \omega^e(\mathbf{x}))$  within  $\mathcal{X}^e$ . Unlike other methods, we avoid strong parametric assumptions about the bias function, relying instead on the multi-task **GP** to extrapolate non-linearly with posterior uncertainty quantification, so that regions with low covariate support naturally exhibit higher uncertainty.

### 3.2. Multi-task Gaussian Processes

A **GP** is a collection of random variables where any finite subset have a joint Gaussian distribution. In the scalar case, the distribution of a **GP**  $f$  is completely specified by its mean function  $m(\mathbf{x}) = \mathbb{E}[f(\mathbf{x})]$  and covariance function  $k(\mathbf{x}, \mathbf{x}') = \mathbb{E}[(f(\mathbf{x}) - m(\mathbf{x}))(f(\mathbf{x}') - m(\mathbf{x}'))]$ . We will assume that  $m(\mathbf{x}) = 0$  throughout. Given a set of observations  $(y_i, \mathbf{x}_i)_{i=1}^n$ , we seek to learn a function  $f$  such that  $y_i = f(\mathbf{x}_i) + \epsilon_i$ , where we assume  $\epsilon_i \sim \mathcal{N}(0, \sigma^2)$ . **GP** regression proceeds by placing a **GP** prior on the function  $f$ , and computing the posterior distribution of  $f$  given the observations.

In our setting, we use a T-learner approach (Künzel et al., 2019) to estimate  $\tau(\mathbf{x})$ , i.e. we individually estimate  $\mathbb{E}[Y^0 \mid \mathbf{x}]$  and  $\mathbb{E}[Y^1 \mid \mathbf{x}]$  with separate models. For brevity, we will focus on  $\mathbb{E}[Y^1 \mid \mathbf{x}]$  in the exposition. We write the study specific response surfaces as:

$$f^e(\mathbf{x}) = \mathbb{E}[Y \mid \mathbf{x}, S = e, A = 1], \quad f^o(\mathbf{x}) = \mathbb{E}[Y \mid \mathbf{x}, S = o, A = 1].$$

For  $\mathbf{f}(\mathbf{x}) = (f^e(\mathbf{x}), f^o(\mathbf{x}))$ , we assign a multi-task **GP** prior  $\mathbf{f} \sim \mathcal{GP}(\boldsymbol{\mu}, K)$ , where  $\boldsymbol{\mu}$  is a bivariate mean function (taken again to be 0) and  $K$  is a positive  $2 \times 2$  matrix-valued covariance function that maps input points  $\mathbf{x}_i$  and  $\mathbf{x}_j$  to matrices quantifying the relationship of the outputs at these inputs. We specify  $K$  in the next section. The key strength of multi-task **GPs** is the ability to share information between tasks, which we will leverage for data fusion. See Appendix **B** Fig 3 for an illustrative comparison to independent **GPs**.

We assume a Gaussian observation model,

$$y_i^e = f^e(\mathbf{x}_i^e) + \epsilon_i^e, \quad y_j^o = f^o(\mathbf{x}_j^o) + \epsilon_j^o,$$

where  $\epsilon_i^e, \epsilon_j^o \sim \mathcal{N}(0, \sigma^2)$  independently across tasks and observations for  $i = 1, \dots, n^e$  and  $j = 1, \dots, n^o$ . For simplicity, we assume a common variance  $\sigma^2$  between tasks but this can be easily extended to task-specific variances. We write  $\mathbf{y}^e$  for the  $n^e$ -vector of outcomes and  $X^e$  for the  $(n^e \times p)$  matrix of covariates respectively, and similarly for the observational dataset.

In data fusion settings for clinical trials, typically  $n^e \ll n^o$ , and  $p(\mathbf{x}^e)$  may not have support over the entire target population. Making inferences across the whole population thus requires some level of extrapolation. We leverage the multi-task GP to improve estimation of  $f^e$  outside the support of  $p(\mathbf{x}^e)$ , given the observations  $(\mathbf{y}^o, X^o)$ . By sharing information between tasks and leveraging the flexible nature of GPs, we hope to increase precision of our estimates without introducing significant bias. The object of interest is the posterior distribution of  $f^e$  given  $\mathcal{D} = (\mathbf{y}^e, X^e, \mathbf{y}^o, X^o)$ , which, by conjugacy, is also a GP. Crucially, the Bayesian framework also provides reliable uncertainty estimates in regions of extrapolation.

### 3.3. Intrinsic coregionalisation models (ICMs)

The **Intrinsic Coregionalization Model (ICM)** is a special case of a multi-task GP with a separable kernel, which is particularly interpretable and suitable for data fusion (Vargas-Guzman and Warrick, 1999). Each task is a linear combination of independent latent functions, yielding a particularly simple covariance structure. For our setting, we have

$$f^e(\mathbf{x}) = \sum_{q=1}^Q \alpha_q^e u_q(\mathbf{x}), \quad f^o(\mathbf{x}) = \sum_{q=1}^Q \alpha_q^o u_q(\mathbf{x}),$$

where  $u_q(\mathbf{x})$  are independent zero-mean latent functions taken from the same scalar GP,  $u_q \sim \mathcal{GP}(0, k)$  for a chosen kernel  $k$ . The scalar coefficients  $(\alpha_q^e, \alpha_q^o)$  are which will be used to construct the coregionalization matrix defined shortly, which governs the dependence structure. The rank of the ICM  $Q$  is the number of independent components, which we set to  $Q = 2$  for the single arm case; we provide a discussion on the interpretation of this later.

The multi-task covariance function can be expressed as

$$K(\mathbf{x}, \mathbf{x}') = B \otimes k(\mathbf{x}, \mathbf{x}'),$$

where  $\otimes$  is the Kronecker product and  $B$  is the coregionalization matrix taking values

$$B = \begin{bmatrix} \beta^e & \beta^{eo} \\ \beta^{eo} & \beta^o \end{bmatrix} = \begin{bmatrix} (\alpha_1^e)^2 + (\alpha_2^e)^2 & \alpha_1^e \alpha_1^o + \alpha_2^e \alpha_2^o \\ \alpha_1^e \alpha_1^o + \alpha_2^e \alpha_2^o & (\alpha_1^o)^2 + (\alpha_2^o)^2 \end{bmatrix}. \quad (1)$$

The posterior distribution over  $f^e$  can then be computed using standard theory (see Appendix C). For a given test point  $\mathbf{x}_*$ , we have that the posterior distribution is Gaussian

$$[f^e(\mathbf{x}_*) \mid \mathcal{D}] \sim \mathcal{N}(m^e(\mathbf{x}_*), V^e(\mathbf{x}_*)),$$

where

$$m^e(\mathbf{x}_*) = k^e(\mathbf{x}_*, X) \Sigma^{-1} \mathbf{y}, \quad V^e(\mathbf{x}_*) = \beta^e k(\mathbf{x}_*, \mathbf{x}_*) - k^e(\mathbf{x}_*, X) \Sigma^{-1} k^e(X, \mathbf{x}_*).$$

Here,  $\mathbf{y} = (\mathbf{y}^e, \mathbf{y}^o)$  and  $X = (X^e, X^o)$  are the concatenated response vectors and covariate matrices respectively, and  $\Sigma = K(X, X) + \sigma^2 I$  with

$$K(X, X) = \begin{bmatrix} \beta^e K(X^e, X^e) & \beta^{eo} K(X^e, X^o) \\ \beta^{eo} K(X^o, X^e) & \beta^o K(X^o, X^o) \end{bmatrix},$$

where  $K(X^s, X^t)$  is the regular (cross-)covariance matrix of the kernel  $k(\mathbf{x}, \mathbf{x}')$  for the covariate matrices from  $S = s$  and  $S = t$ . We similarly have

$$k^e(\mathbf{x}_*, X) = [\beta^e k(\mathbf{x}_*, X^e) \quad \beta^{eo} k(\mathbf{x}_*, X^o)],$$

where  $k(\mathbf{x}_*, X^s)$  is the row vector of covariances between  $\mathbf{x}_*$  and  $X^s$ , and  $k^e(X, \mathbf{x}_*) = k^e(\mathbf{x}_*, X)^T$ . Given this posterior,  $m^e(\mathbf{x}_*)$  provides point estimates of the response surface, with associated posterior variance  $V^e(\mathbf{x}_*)$  which can be used to compute credible intervals.

### 3.4. Causal-ICM

We now introduce *Causal-ICM*. Specifically, we propose an interpretable parametrisation of the **ICM** for causal inference and introduce a bespoke procedure for learning its coefficients, rather than relying on standard marginal likelihood maximisation. This serves to control the influence of the observational dataset and avoid “swamping” the **RCT** data. *Causal-ICM* consists of the following choices for the ICM coefficients:

$$\begin{bmatrix} \alpha_1^e & \alpha_2^e \\ \alpha_1^o & \alpha_2^o \end{bmatrix} = \begin{bmatrix} 1 & 0 \\ \rho & \sqrt{1 - \rho^2} \end{bmatrix}$$

Under this parameterization,  $\rho \in (0, 1)$  controls the degree of borrowing, with  $\rho \rightarrow 1$  corresponding to maximum borrowing and  $\rho \rightarrow 0$  to none (We provide an additional interpretation of  $\rho$  in Appendix D, Proposition 2). Although this implies  $\beta^e = \beta^o = 1$  (and  $\beta_{eo} = \rho$ ), the model remains flexible as long as the kernel  $k(\mathbf{x}, \mathbf{x})$  includes an independent scaling term (e.g., the variance in an RBF kernel) and the scales of  $f^e$  and  $f^o$  are similar.

With these suggested settings for the ICM coefficients, we then have:

$$f^e(\mathbf{x}) = u_1(\mathbf{x}), \quad f^o(\mathbf{x}) = \rho f^e(\mathbf{x}) + \sqrt{1 - \rho^2} u_2(\mathbf{x}).$$

Thus,  $f^e = u_1$  and  $f^o$  is a scaled version of  $f^e$  plus a term capturing confounding. Choosing a positive  $\rho \in (0, 1)$  is reasonable, as  $f^o(\mathbf{x})$  is expected to be highly correlated with  $f^e(\mathbf{x})$  - both model the conditional expectation of the outcome - with  $f^o$  additionally contaminated by confounding. In practice, restricting  $\alpha_2^o$  minimally affects flexibility while improving interpretability. Remaining hyperparameters, including kernel parameters and sampling variance, are estimated via marginal likelihood maximisation.

#### 3.4.1. VARIANCE BOUND FOR CONDITIONAL MEAN FUNCTION UNDER CAUSAL-ICM

When evaluating treatment effects, it is important to quantify uncertainty alongside point estimates. The multi-task Gaussian process naturally provides this uncertainty via the posterior variance  $V^e(\mathbf{x}_*)$ . In data fusion, a key concern is that large observational samples may “swamp” the experimental data, yielding biased and overconfident estimates of  $\tau(\mathbf{x})$ .

*Causal-ICM* mitigates this, as shown by a lower bound on the posterior variance  $V^e(\mathbf{x}_*)$  even as  $n^o$  grows. This variance bound can also be seen as formally limiting the information flow from the observational dataset, similar to cut models (Lin et al., 2025a).

**Proposition 1** *Suppose  $\mathbf{x}_*$  is a test point of interest. Let  $V^e(\mathbf{x}_*)$  and  $V_{\mathcal{D}_e}^e(\mathbf{x}_*)$  denote the posterior variances of  $f^e(\mathbf{x}_*)$  given the full dataset  $\mathcal{D} = (\mathbf{y}^e, X^e, \mathbf{y}^o, X^o)$  and the experimental dataset  $\mathcal{D}_e = (\mathbf{y}^e, X^e)$  only respectively. The posterior variance given  $\mathcal{D}$  then satisfies*

$$V^e(\mathbf{x}_*) \geq (1 - \rho^2) V_{\mathcal{D}_e}^e(\mathbf{x}_*) \tag{2}$$

where  $\rho \in (0, 1)$  is the borrowing hyperparameter.

**Proof** Let  $n^e, n^o \geq 0$  denote the sizes of the experimental and observational datasets respectively. We outline the proof for  $n^e = 0$  here, which corresponds to the prior-only case for the RCT. The proof for the general case  $n^e > 0$  is deferred to Appendix E. The key is that when  $n^e = 0$ , the posterior variance can be written as

$$V^e(\mathbf{x}_*) = (1 - \rho^2) k(\mathbf{x}_*, \mathbf{x}_*) + \rho^2 V_{\mathcal{D}_o}^e(\mathbf{x}_*)$$

where  $V_{\mathcal{D}_o}^e$  is the posterior variance for a GP with kernel  $k(\mathbf{x}, \mathbf{x})$  fit only to  $\mathcal{D}_o = (\mathbf{y}^o, X^o)$ , and  $k(\mathbf{x}_*, \mathbf{x}_*)$  is the prior variance. As  $V_{\mathcal{D}_o}^e(\mathbf{x}_*) \geq 0$ , we obtain the desired lower bound. ■

An intuitive understanding of the result is as follows: for two random variables with correlation  $\rho$ , knowledge of one random variable does not inform us of the exact value of the other unless  $\rho = 1$ . The key interpretation of Proposition 1 in the data fusion context is as follows: even as  $n^o \rightarrow \infty$ , the posterior variance of  $f^e(\mathbf{x}_*)$  conditional on the full dataset will at most decrease by a factor of  $(1 - \rho^2)$  relative to the posterior variance given the experimental data only, where  $|\rho| \leq 1$ . We conjecture that this inequality is tight as  $n^o \rightarrow \infty$ . This can be interpreted as limiting the ‘effective sample size’ of the observational dataset to be  $1/(1 - \rho^2)$  relative to the experimental dataset. Crucially, this variance bound protects from having very tight credible intervals centred around a biased estimate - the posterior uncertainty will accurately reflect our distrust of the observational dataset. We also expect this ‘effective sample size’ effect to hold for the posterior mean of  $f^e(\mathbf{x}_*)$ , where there the bias introduced to the posterior mean by  $\mathcal{D}_o$  is limited again by the choice of  $\rho$ . We leave this interesting direction for future work. Although our focus is on the conditional mean functions, our approach also provides the posterior distribution of the confounding function, offering additional insights that may be of independent interest (see Appendix F).

### 3.4.2. TUNING $\rho$

We now outline a data-adaptive procedure to select  $\rho$ , where the goal is to prevent information from the large confounded observational study from swamping that of the smaller unconfounded RCT. Our proposal is based on cross-validation to minimize the **Root Mean Squared Error (RMSE)** on weighted held-out RCT patients only, where the weighting tailors  $\rho$  for extrapolation. Specifically, use 5-fold cross-validation, as the RCT sample size is usually

small, and we consider  $\rho \in [0.0, 0.1, \dots, 1.0]$  on a grid. In particular, we minimize the following objective:

$$\mathcal{L}(\rho) = \sum_{i=1}^{n_{\text{held-out}}} w(\tilde{\mathbf{x}}_i) (\tilde{y}_i - m^e(\tilde{\mathbf{x}}_i))^2, \quad w(\mathbf{x}) = \frac{1}{1 - p(S = 0 \mid \mathbf{x})}$$

where  $\{\tilde{y}_i, \tilde{\mathbf{x}}_i\}_{i=1}^{n_{\text{held-out}}}$  is a held-out subset of  $(\mathbf{y}^e, X^e)$  that was not used to train  $m^e$ . The above objective is motivated as follows. Firstly, we only evaluate predictions on RCT patients where there is no confounding present. Secondly, the weights will upweight RCT patients who have higher probability of arising from the observational dataset, so  $\rho$  will be tailored to improve extrapolation beyond the RCT support. We then expect the largest gains in power of  $\rho$  is chosen close to 1, indicating that the confounding effect is small. We will see in the experiments that this works well in practice.

### 3.4.3. EXTENSION TO CATE ESTIMATION

When both treatment and control arms are available, we fit two separate rank-2 ICMs to model  $(f_0^e, f_0^o)$  and  $(f_1^e, f_1^o)$ , focusing on sharing information between the experimental and observational datasets. This yields independent posteriors for  $f_0^e$  and  $f_1^e$ , which we combine to obtain the posterior of  $\tau(\mathbf{x})$  by differencing the means and summing the variances. We allow distinct kernel hyperparameters for the two ICMs while using a common  $\rho$ , chosen to minimise the average  $\mathcal{L}(\rho)$  across treatment groups. This setup corresponds to a T-learner approach (Künzel et al., 2019).

## 4. Experiments

We investigated *Causal-ICM*'s performance through multiple simulation studies and a comprehensive analysis of Real-World Data (RWD) sourced from the Tennessee STAR study (Achilles et al., 2008). The code will be made available online. The optimal value of  $\rho$  is chosen data-adaptively in all cases (Section 3.4.2). Model evaluation and comparison were based on the RMSE, averaged over the covariate distribution of the observational study.

We compared *Causal-ICM* against several benchmarks: (i) a T-learner with GPs regressors trained separately on each study, (ii) the two-step method of Kallus et al. (2018), which debiases observational data via a low-complexity bias function with GPs as base learners, (iii) the integrative estimator of Yang et al. (2022b), which assumes a non-linear CATE and linear confounding effect, (iv) the power likelihood method of Lin and Evans (2023), and (v) the test-then-pool approach of Yang et al. (2022a). For Yang et al. (2022b), we used the default settings recommended in their paper, while for Lin and Evans (2023), we selected the power parameter  $\eta$  by maximizing the Expected Log Pointwise Predictive Density (ELPD), which in both cases resulted in  $\eta = 0$  (no pooling). Finally, we assessed the coverage of *Causal-ICM*'s CATE credible intervals across simulation scenarios, comparing them with those from the T-learner approaches.

We used GPy (2012) to train the ICMs, with  $\rho$  tuned as described in Section 3.4.2 and remaining hyperparameters estimated via marginal likelihood maximisation. All experiments were run on a single Macbook Pro (M2) with 16GB RAM.

### 4.1. Simulation Studies

We showcase the performance of *Causal-ICM* in the main text using two distinct simulation studies. Further simulation studies, both univariate and multivariate, are detailed in Appendix A.8, illustrating the competitive performance of *Causal-ICM* in a wide range of settings, including both linear and non-linear scenarios for the potential outcomes, CATE and confounding function. In all simulations, the sample size is roughly between 200-300 for the RCT and 1000 for the observational study.

In the first simulation setting, we assume a continuous baseline covariate  $X \sim \text{Unif}[-2, 2]$ . The values of  $X$  control the trial participation probability, where  $S \sim \text{Bernoulli}(p_S)$  for  $p_S = \exp(-3 - 3X)/(1 + \exp(-3 - 3X))$ . Here, patients with smaller  $X$  values have higher probability of being assigned in the trial. After selecting all trial participants, we assign them randomly to treatment with  $A \sim \text{Bernoulli}(0.5)$ . The observed outcomes are generated as  $Y = A\tau(X) + X + \epsilon$  for  $A \in \{0, 1\}$ , where  $\tau(X) = 1 + X$  is the CATE and  $\epsilon \sim \mathcal{N}(0, 1)$ . For the observational study we have  $X \sim \text{Unif}[-2, 2]$  and the treatment is generated according to  $A \sim \text{Bernoulli}(e(X))$  where  $\text{logit}(e(X)) = -X$ . Similarly to the trial, the observed outcomes are  $Y = A\tau(X) + X + U + \epsilon$  for  $A \in \{0, 1\}$ . Here,  $U$  is the hidden confounder which is generated from  $U \sim \mathcal{N}((2A - 1)X, 1)$ , yielding a linear confounding effect  $\eta(X) = 2X$ . In the second simulation, we change the potential outcomes, the CATE and the confounding effect to be non-linear as follows:  $Y = A\tau(X) + X^2 - 1 + U + \epsilon$ , where  $\tau(X) = 1 + X + X^2$  and  $U \sim \mathcal{N}((2A - 1)\sin(X - 1), 1)$ , yielding  $\eta(X) = 2\sin(X - 1)$ . All other variables remain the same.

Under a linear CATE and a linear unobserved confounding effect, *Causal-ICM* (with  $\rho = 0.1$ ) exhibited comparable performance to the integrative HTE estimator (Yang et al. (2022b)) and the Elastic HTE estimator of Yang et al. (2022a), and superior performance to all other techniques (Fig 1 left). In the non-linear setting (both CATE and unobserved confounding effect), *Causal-ICM* outperformed all other methods yielding the lowest RMSE (Fig 1 right). These results reflect the limitations of the experimental grounding, the Integrative HTE and the Elastic HTE methods. Each of these are designed for linear treatment or confounding effect, resulting in inflated RMSE values in scenarios where these assumptions do not hold. In the multivariate setting *Causal-ICM* performed equally good or better than most methods, being outperformed by parametric approaches only when the model was correctly specified (see Appendix G.2 Fig 4).

Regarding uncertainty quantification, our approach generated 95% credible intervals with reasonable, though slightly conservative, coverage close to the nominal level in both simulation settings (Fig 2). The observational-only T-learner had the lowest coverage across the baseline covariate support, which is expected since its estimates are biased but exhibit lower uncertainty due to the larger dataset. This is exactly the behaviour that *Causal-ICM* is robust to, as formalized in Proposition 1: the large sample size of the observational study does not overwhelm the *Causal-ICM*'s estimates. See Figure 5 in Appendix H for an illustrative example of extrapolation and uncertainty quantification with *Causal-ICM* in the second simulation setting. Additionally, the *Causal-ICM* is robust against the kernel choice (see Appendix I Table 3), the observational sample size (see Appendix I Table 4), and the degree of overlap between the two studies (see Appendix I Table 5), yielding similar RMSE

values under all these different scenarios. Finally, the choice of  $\rho$  plays an important role in controlling the influence of the confounded observational data (see Appendix I Table 2).

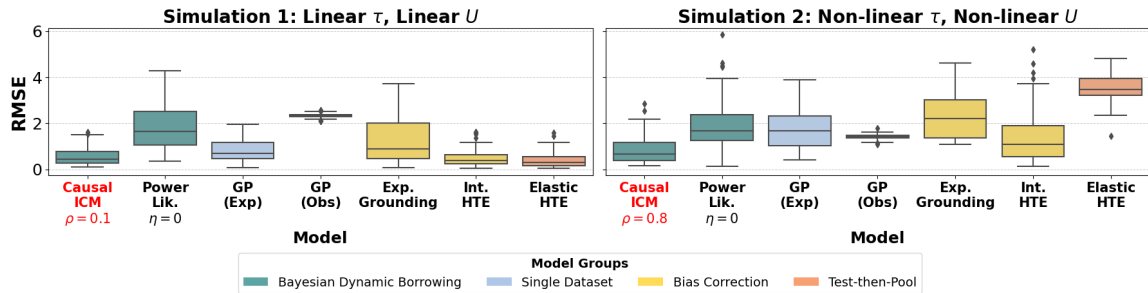


Figure 1: Simulation results over 100 simulated datasets. *Left*: Simulation setting 1: linear [CATE](#) and unobserved confounding, *Right*: Non-linear [CATE](#) and unobserved confounding

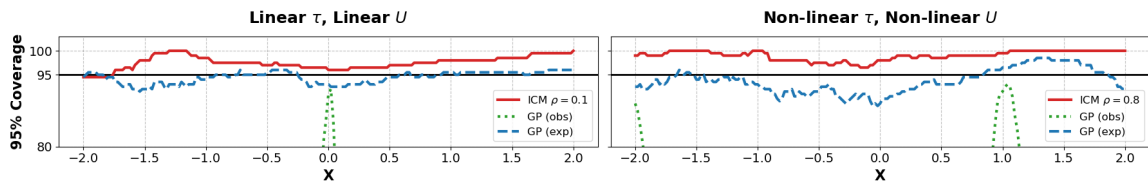


Figure 2: 95% conditional coverage over the covariate distribution of the observational study for the two simulation studies. The black solid line indicates the nominal level (95%). *Left*: First simulation setting (linear [CATE](#) and confounding), *Right*: Second simulation setting (non-linear [CATE](#) and confounding). The GP (obs) method exhibited 0% coverage in most of the support covariate distribution.

## 4.2. Real-World Data Analysis

The Tennessee Student/Teacher Achievement Ratio (STAR) ([Achilles et al., 2008](#)) randomised experiment initiated in 1985 studied the impact of class size on student outcomes through standardized test scores from first to third grade. We focus on two ‘treatments’, here corresponding to two experimental conditions: small class size and regular class size. We followed a similar approach to [Kallus et al. \(2018\)](#) and used the real data to produce a ‘confounded’ dataset, corresponding to the observational sample, and a smaller unconfounded dataset, which comprised our [RCT](#) data. After removing subjects with missing treatment or outcome values, we were left with a randomised sample of 4218 students. Baseline covariates included gender, race, birth month, birth year, free lunch eligibility and teacher ID. To obtain the ‘experimental’ dataset we sampled randomly only from rural or inner city students. To form the confounded observational dataset, we aggregated all control cases not included in the experimental data. Additionally, for those undergoing treatment, we drew a sample with a down-weighting mechanism applied to individuals whose outcomes fell below the 30<sup>th</sup> percentile. After preprocessing, the unconfounded dataset included 422 students, while the confounded dataset included 2593. Further, 379 students were kept as a validation set. We compared *Causal-ICM* (optimal  $\rho = 0.4$ ) with a [GP](#) based T-learner trained either on the

experimental or the observational data, the experimental grounding method of [Kallus et al. \(2018\)](#) either with Random Forest or GP as base learners and the Integrative HTE method of [Yang et al. \(2022b\)](#). We were unable to include the Elastic HTE estimator ([Yang et al. \(2023\)](#)) or the power likelihood approach ([Lin et al. \(2025a\)](#)), as both methods encountered convergence issues due to the datasets’ high dimensionality and the limited variability in their categorical covariates.

In order to compare *Causal-ICM* with existing methods, we require a notion of ground truth. Given the randomised nature of the study, we assume that an unbiased estimate of the [CATE](#) can be obtained using a doubly robust estimator, which we then treat as the ground truth. To obtain this, we estimated the propensity score and conditional expectation models using the full dataset, prior to splitting it into the confounded and unconfounded samples ([Saito and Yasui, 2020](#)). We note that, in the absence of the true [CATE](#), other performance metrics adapted to the counterfactual nature of the evaluation are also available ([Alaa and Van Der Schaar, 2019](#); [Boyer et al., 2023](#)).

The results are summarised in [Table 1](#) below. *Causal-ICM* again performed highly competitively in terms of RMSE, on a par with the experimental grounding method with Random Forests as base learners.

Table 1: RMSE values for the RWD example. *Causal-ICM*: our method; GP (exp): T-learner with GPs as base learners trained in the unconfounded; GP (obs): T-learner with GPs as base learners trained in the confounded data; Experimental grounding (GP): the method proposed by [Kallus et al. \(2018\)](#) with GPs as base learners; Experimental grounding (RF): the method proposed by [Kallus et al. \(2018\)](#) with Random Forest as base learners; Integrative HTE: the method proposed by [Yang et al. \(2022b\)](#)

Method	RMSE	Method	RMSE
<i>Causal-ICM</i> ( $\rho = 0.4$ )	<b>6.29</b>	Experimental grounding (GP)	6.38
GP (exp)	6.36	Experimental grounding (RF)	<b>6.27</b>
GP (obs)	7.47	Integrative HTE	11.84

## 5. Discussion

We have developed *Causal-ICM*, a rank-2 [ICM](#) to combine observational and experimental data to estimate treatment effects for a target population, where the hyperparameter  $\rho$  controls the degree of borrowing in an interpretable way. In contrast to existing methods, *Causal-ICM* is highly flexible and does not make any assumptions about the functional form of the [CATE](#) or the effect of unobserved confounding. By providing accurate estimates of heterogeneous treatment effects, *Causal-ICM* has the potential to inform more personalised medical decision making. Moreover, unlike other data fusion methods, *Causal-ICM* is able to provide uncertainty quantification. By identifying regions of the population where treatment effects remain highly uncertain, our approach can help guide the design of future trials to improve representativeness and reduce uncertainty to satisfactory levels ([Yang et al. \(2025\)](#)).

Despite the inherent difficulty of extrapolation, *Causal-ICM* appears to extrapolate well, achieving reliable levels of coverage. In general, it is challenging to ensure frequentist coverage for Bayesian nonparametric methods, which is a limitation of our approach. Another limitation

is the sensitivity of uncertainty estimates to the kernel choice and the hyperparameter optimization, which is an intrinsic challenge of GPs. Future research directions for *Causal-ICM* include extensions to multiple data sources or treatment arms, placing a prior on the parameter  $\rho$ , and incorporating the propensity score into the model. Investigating partial identification of causal effects, especially in regions of extrapolation, is also important Pfister and Bühlmann (2024). Methodological extensions such as allowing distinct kernels for the latent functions, accommodating non-Gaussian likelihoods, and improving computational scalability via sparse GPs or inducing points represent additional promising directions (see Appendix J).

## References

- C.M. Achilles, Helen Pate Bain, Fred Bellott, Jayne Boyd-Zaharias, Jeremy Finn, John Folger, John Johnston, and Elizabeth Word. Tennessee’s Student Teacher Achievement Ratio (STAR) project, April 2008. URL <http://arxiv.org/abs/1106.6251>.
- Ahmed Alaa and Mihaela Van Der Schaar. Validating causal inference models via influence functions. In Kamalika Chaudhuri and Ruslan Salakhutdinov, editors, *Proceedings of the 36th International Conference on Machine Learning*, volume 97 of *Proceedings of Machine Learning Research*, pages 191–201. PMLR, 09–15 Jun 2019. URL <https://proceedings.mlr.press/v97/aaa19a.html>.
- Ahmed M. Alaa and Mihaela van der Schaar. Bayesian Inference of Individualized Treatment Effects using Multi-task Gaussian Processes. In *Advances in Neural Information Processing Systems*, volume 30. Curran Associates, Inc., 2017. URL <https://proceedings.neurips.cc/paper/2017/hash/6a508a60aa3bf9510ea6acb021c94b48-Abstract.html>.
- Mauricio A. Alvarez, Lorenzo Rosasco, and Neil D. Lawrence. Kernels for Vector-Valued Functions: a Review, April 2012. URL <http://arxiv.org/abs/1106.6251>. arXiv:1106.6251 [cs, math, stat].
- Christopher B. Boyer, Issa J. Dahabreh, and Jon A. Steingrimsson. Assessing model performance for counterfactual predictions, 2023.
- Carly Lupton Brantner, Ting-Hsuan Chang, Trang Quynh Nguyen, Hwanhee Hong, Leon Di Stefano, and Elizabeth A. Stuart. Methods for Integrating Trials and Non-Experimental Data to Examine Treatment Effect Heterogeneity, March 2023. URL <http://arxiv.org/abs/2302.13428>. arXiv:2302.13428 [stat].
- Alberto Caron, Ioanna Manolopoulou, and Gianluca Baio. Counterfactual Learning with Multioutput Deep Kernels. *Transactions on Machine Learning Research*, 2022. ISSN 2835-8856. URL <https://openreview.net/forum?id=iGREAJdULX>.
- Bénédicte Colnet, Imke Mayer, Guanhua Chen, Awa Dieng, Ruohong Li, Gaël Varoquaux, Jean-Philippe Vert, Julie Josse, and Shu Yang. Causal inference methods for combining randomized trials and observational studies: a review, January 2023. URL <http://arxiv.org/abs/2011.08047>. arXiv:2011.08047 [stat].

- Issa J. Dahabreh and Miguel A. Hernán. Extending inferences from a randomized trial to a target population. *European Journal of Epidemiology*, 34(8):719–722, August 2019. ISSN 1573-7284. doi: 10.1007/s10654-019-00533-2.
- Irina Degtiar and Sherri Rose. A review of generalizability and transportability. *Annual Review of Statistics and Its Application*, 10(1):501–524, 2023. doi: 10.1146/annurev-statistics-042522-103837. URL <https://doi.org/10.1146/annurev-statistics-042522-103837>.
- Ilker Demirel, Ahmed Alaa, Anthony Philippakis, and David Sontag. Prediction-powered generalization of causal inferences, 2024. URL <https://arxiv.org/abs/2406.02873>.
- Jake Fawkes, Michael O’Riordan, Athanasios Vlontzos, Oriol Corcoll, and Ciarán Mark Gilligan-Lee. The hardness of validating observational studies with experimental data. In Yingzhen Li, Stephan Mandt, Shipra Agrawal, and Emtiyaz Khan, editors, *Proceedings of The 28th International Conference on Artificial Intelligence and Statistics*, volume 258 of *Proceedings of Machine Learning Research*, pages 1819–1827. PMLR, 03–05 May 2025. URL <https://proceedings.mlr.press/v258/fawkes25b.html>.
- Thomas R. Frieden. Evidence for health decision making — beyond randomized, controlled trials. *New England Journal of Medicine*, 377(5):465–475, 2017. doi: 10.1056/NEJMra1614394. URL <https://www.nejm.org/doi/full/10.1056/NEJMra1614394>.
- AmirEmad Ghassami, Chang Liu, Alan Yang, David Richardson, Ilya Shpitser, and Eric Tchetgen Tchetgen. Combining experimental and observational data for identification and estimation of long-term causal effects, 2025. URL <https://arxiv.org/abs/2201.10743>.
- GPpy. GPpy: A Gaussian process framework in Python. <http://github.com/SheffieldML/GPy>, 2012.
- P. Richard Hahn, Jared S. Murray, and Carlos M. Carvalho. Bayesian Regression Tree Models for Causal Inference: Regularization, Confounding, and Heterogeneous Effects (with Discussion). *Bayesian Analysis*, 15(3):965–1056, September 2020. ISSN 1936-0975, 1931-6690. doi: 10.1214/19-BA1195. Publisher: International Society for Bayesian Analysis.
- Tobias Hatt, Jeroen Berrevoets, Alicia Curth, Stefan Feuerriegel, and Mihaela van der Schaar. Combining Observational and Randomized Data for Estimating Heterogeneous Treatment Effects, February 2022. URL <http://arxiv.org/abs/2202.12891>. arXiv:2202.12891 [cs, stat].
- Bin Huang, Chen Chen, Jinzhong Liu, and Siva Sivaganisan. Gpmatch: A bayesian causal inference approach using gaussian process covariance function as a matching tool. *Frontiers in Applied Mathematics and Statistics*, 9, 2023. ISSN 2297-4687. doi: 10.3389/fams.2023.1122114. URL <https://www.frontiersin.org/articles/10.3389/fams.2023.1122114>.
- Guido Imbens, Nathan Kallus, Xiaojie Mao, and Yuhao Wang. Long-term causal inference under persistent confounding via data combination, 2024. URL <https://arxiv.org/abs/2202.07234>.

- Nathan Kallus, Aahlad Manas Puli, and Uri Shalit. Removing Hidden Confounding by Experimental Grounding. In *Advances in Neural Information Processing Systems*, volume 31. Curran Associates, Inc., 2018. URL <https://papers.nips.cc/paper/2018/hash/566f0ea4f6c2e947f36795c8f58ba901-Abstract.html>.
- Sören R. Künzel, Jasjeet S. Sekhon, Peter J. Bickel, and Bin Yu. Metalearners for estimating heterogeneous treatment effects using machine learning. *Proceedings of the National Academy of Sciences*, 116(10):4156–4165, February 2019. ISSN 1091-6490. doi: 10.1073/pnas.1804597116. URL <http://dx.doi.org/10.1073/pnas.1804597116>.
- Quinn Lanners, Cynthia Rudin, Alexander Volfovsky, and Harsh Parikh. Data fusion for partial identification of causal effects, 2025. URL <https://arxiv.org/abs/2505.24296>.
- Xi Lin and Robin J. Evans. Many Data: Combine Experimental and Observational Data through a Power Likelihood, April 2023. URL <http://arxiv.org/abs/2304.02339>. arXiv:2304.02339 [math, stat].
- Xi Lin, Jens Magelund Tarp, and Robin J. Evans. Data fusion for efficiency gain in ate estimation: A practical review with simulations, 2024. URL <https://arxiv.org/abs/2407.01186>.
- Xi Lin, Jens Magelund Tarp, and Robin J. Evans. Combining experimental and observational data through a power likelihood. *Biometrics*, 81(1):ujaf008, 2025a. doi: 10.1093/biomtc/ujaf008.
- Xi Lin, Jens Magelund Tarp, and Robin J. Evans. Combining experimental and observational data through a power likelihood. *Biometrics*, 81(1):ujaf008, 2025b. doi: 10.1093/biomtc/ujaf008.
- National Academies of Sciences, Engineering, and Medicine. *Improving Representation in Clinical Trials and Research: Building Research Equity for Women and Underrepresented Groups*. The National Academies Press, Washington, DC, 2022. ISBN 978-0-309-27820-1. doi: 10.17226/26479. URL <https://nap.nationalacademies.org/catalog/26479/improving-representation-in-clinical-trials-and-research-building-research-equity>.
- Niklas Pfister and Peter Bühlmann. Extrapolation-aware nonparametric statistical inference, 2024. URL <https://arxiv.org/abs/2402.09758>.
- Yuta Saito and Shota Yasui. Counterfactual cross-validation: Stable model selection procedure for causal inference models, 2020.
- Xu Shi, Ziyang Pan, and Wang Miao. Data integration in causal inference. *Wiley Interdisciplinary Reviews: Computational Statistics*, 15(1):e1581, 2023. doi: 10.1002/wics.1581.
- J.A. Vargas-Guzman and A.W. Warrick. Geostatistics for natural resources evaluation. *Journal of Environmental Quality*, 28(3):1044–1044, 1999. doi: <https://doi.org/10.2134/jeq1999.00472425002800030046x>. URL <https://access.onlinelibrary.wiley.com/doi/abs/10.2134/jeq1999.00472425002800030046x>.

Stefan Wager and Susan Athey. Estimation and Inference of Heterogeneous Treatment Effects using Random Forests. *Journal of the American Statistical Association*, 113(523):1228–1242, July 2018. ISSN 0162-1459. doi: 10.1080/01621459.2017.1319839. URL <https://doi.org/10.1080/01621459.2017.1319839>. Publisher: Taylor & Francis \_eprint: <https://doi.org/10.1080/01621459.2017.1319839>.

Sam Witty, Kenta Takatsu, David Jensen, and Vikash Mansinghka. Causal inference using gaussian processes with structured latent confounders. In *Proceedings of the 37th International Conference on Machine Learning*, ICML’20. JMLR.org, 2020.

Lili Wu and Shu Yang. Integrative  $R$ -learner of heterogeneous treatment effects combining experimental and observational studies. In *Proceedings of the First Conference on Causal Learning and Reasoning*, pages 904–926. PMLR, June 2022. URL <https://proceedings.mlr.press/v177/wu22a.html>. ISSN: 2640-3498.

Shu Yang, Chenyin Gao, Donglin Zeng, and Xiaofei Wang. Elastic Integrative Analysis of Randomized Trial and Real-World Data for Treatment Heterogeneity Estimation, November 2022a. URL <http://arxiv.org/abs/2005.10579>. arXiv:2005.10579 [stat].

Shu Yang, Donglin Zeng, and Xiaofei Wang. Improved Inference for Heterogeneous Treatment Effects Using Real-World Data Subject to Hidden Confounding, January 2022b. URL <http://arxiv.org/abs/2007.12922>. arXiv:2007.12922 [stat].

Shu Yang, Chenyin Gao, Donglin Zeng, and Xiaofei Wang. Elastic integrative analysis of randomised trial and real-world data for treatment heterogeneity estimation. *Journal of the Royal Statistical Society. Series B: Statistical Methodology*, 85(3):575–596, 2023. doi: 10.1093/jrsssb/qkad017.

Shu Yang, Margaret Gamalo, and Haoda Fu. Integrating rcts, rwd, ai/ml and statistics: Next-generation evidence synthesis, 2025. URL <https://arxiv.org/abs/2511.19735>.

## Appendix A. Identification of **CATE** in the RCT

Below we show that the **CATE** can be identified using observed data in the **RCT**.

$$\begin{aligned}
 \mathbb{E}[Y^1 - Y^0 \mid \mathbf{X}_\tau] &= \mathbb{E}[\mathbb{E}[Y^1 - Y^0 \mid \mathbf{X}_\tau \cup \mathbf{X}_S] \mid \mathbf{X}_\tau] \\
 &\quad \text{(tower property)} \\
 &= \mathbb{E}[\mathbb{E}[Y^1 - Y^0 \mid \mathbf{X}_\tau \cup \mathbf{X}_S, S = e] \mid \mathbf{X}_\tau] \\
 &\quad \text{(Assumptions A4)} \\
 &= \mathbb{E}[\mathbb{E}[Y^1 \mid A = 1, \mathbf{X}_\tau \cup \mathbf{X}_S, S = e] - \mathbb{E}[Y^0 \mid A = 0, \mathbf{X}_\tau \cup \mathbf{X}_S, S = e] \mid \mathbf{X}_\tau] \\
 &\quad \text{(Assumptions A2)} \\
 &= \mathbb{E}[\mathbb{E}[Y^1 \mid A = 1, \mathbf{X}_\tau \cup \mathbf{X}_S, S = e] \mid \mathbf{X}_\tau] - \mathbb{E}[\mathbb{E}[Y^0 \mid A = 0, \mathbf{X}_\tau \cup \mathbf{X}_S, S = e] \mid \mathbf{X}_\tau] \\
 &\quad \text{(linearity of conditional expectation)} \\
 &= \mathbb{E}[\mathbb{E}[Y \mid A = 1, \mathbf{X}_\tau \cup \mathbf{X}_S, S = e] \mid \mathbf{X}_\tau] - \mathbb{E}[\mathbb{E}[Y \mid A = 0, \mathbf{X}_\tau \cup \mathbf{X}_S, S = e] \mid \mathbf{X}_\tau] \\
 &\quad \text{(Assumption A1)} \\
 &= \mathbb{E}[Y \mid A = 1, \mathbf{X}_\tau, S = e] - \mathbb{E}[Y \mid A = 0, \mathbf{X}_\tau, S = e] \\
 &\quad \text{(tower property)}
 \end{aligned}$$

## Appendix B. Illustrative example

Figure 3 depicts the differences between single independent GPs and multi-task GPs. Independent GPs excel in regions with observed data but exhibit suboptimal performance during extrapolation. In contrast, Multitask GPs enhance both prediction accuracy and uncertainty quantification in unobserved areas, showcasing superior performance in extrapolation scenarios.

## Appendix C. Derivation of Posterior Distribution

The ICM set-up is

$$\begin{aligned}
 f^e(\mathbf{x}) &= \alpha_1^e u_1(\mathbf{x}) + \alpha_2^e u_2(\mathbf{x}) \\
 f^o(\mathbf{x}) &= \alpha_1^o u_1(\mathbf{x}) + \alpha_2^o u_2(\mathbf{x})
 \end{aligned}$$

where  $u_i(\mathbf{x}) \sim \mathcal{GP}(0, k(\mathbf{x}, \mathbf{x}))$  independently. Suppose we observe  $(\mathbf{y}^e, X^e)$  and  $(\mathbf{y}^o, X^o)$ , where the dataset is of size  $n_e$  and  $n_o$  respectively. The observational model is

$$\begin{aligned}
 y_i^e &= f^e(\mathbf{x}_i) + \epsilon_i^e \\
 y_i^o &= f^o(\mathbf{x}_i) + \epsilon_i^o
 \end{aligned}$$

where both  $\epsilon^e, \epsilon^o$  arise independently from  $\mathcal{N}(0, \sigma^2)$ .

We clearly have  $\mathbb{E}[y_i^e] = \mathbb{E}[y_i^o] = 0$ , where the expectation is over both the observation noise and the GP prior. The variance is more interesting. It is not difficult to show that

$$\mathbb{E}[y_i^e y_j^e] = \begin{cases} \beta^e k(\mathbf{x}_i^e, \mathbf{x}_j^e) + \sigma^2 & \text{if } i = j \\ \beta^e k(\mathbf{x}_i^e, \mathbf{x}_j^e) & \text{otherwise} \end{cases}$$

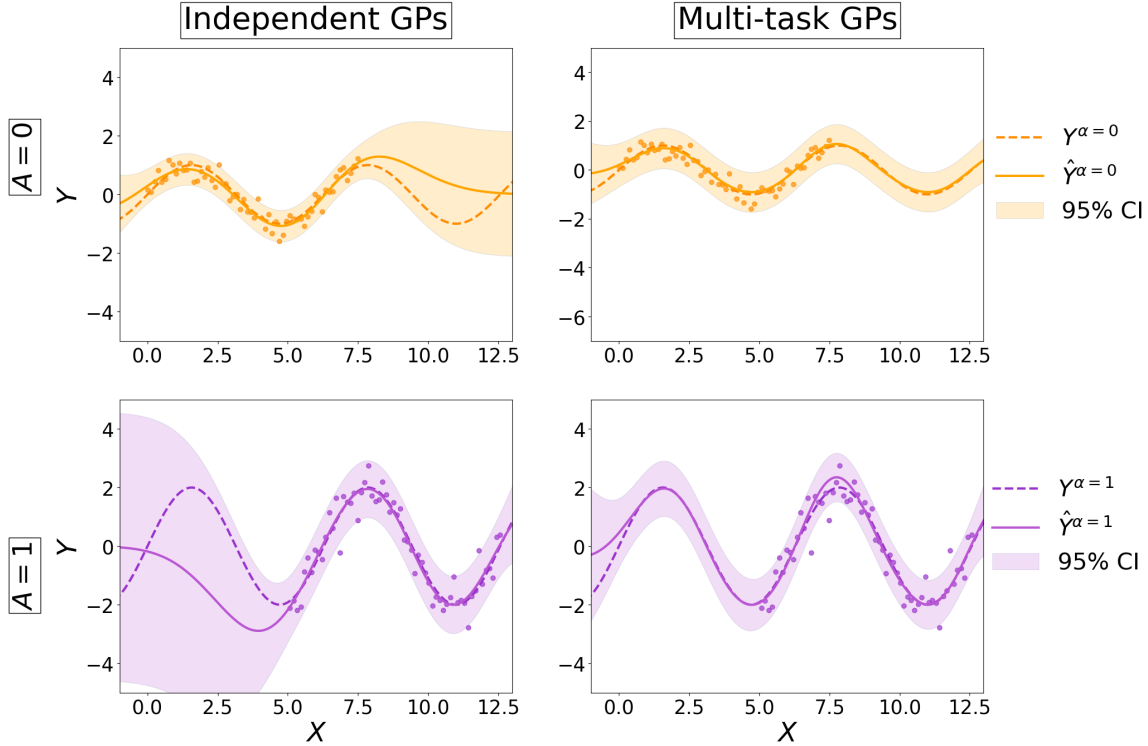


Figure 3: Comparative illustration between Independent GPs and Multitask GP. Here,  $A$  represents distinct treatment groups,  $Y$  corresponds to the outcome, and  $X$  denotes baseline covariates.

Similarly, we have

$$\mathbb{E}[y_i^o y_j^o] = \begin{cases} \beta^o k(\mathbf{x}_i^o, \mathbf{x}_j^o) + \sigma^2 & \text{if } i = j \\ \beta^o k(\mathbf{x}_i^o, \mathbf{x}_j^o) & \text{otherwise} \end{cases}$$

Finally, we have

$$\mathbb{E}[y_i^e y_j^o] = \beta^{eo} k(\mathbf{x}_i^e, \mathbf{x}_j^o).$$

Consider a new test point  $\mathbf{x}_*$ , and we are interested in  $f^e(\mathbf{x}_*)$  and  $f^o(\mathbf{x}_*)$ . One can also show that  $\mathbb{E}[f^e(\mathbf{x}_*)] = \mathbb{E}[f^o(\mathbf{x}_*)] = 0$ , and

$$\begin{aligned} \mathbb{E}[f^e(\mathbf{x}_*) y_i^e] &= \beta^e k(\mathbf{x}_i^e, \mathbf{x}_*) \\ \mathbb{E}[f^o(\mathbf{x}_*) y_i^o] &= \beta^o k(\mathbf{x}_i^o, \mathbf{x}_*) \\ \mathbb{E}[f^e(\mathbf{x}_*) y_i^o] &= \beta^{eo} k(\mathbf{x}_i^o, \mathbf{x}_*) \\ \mathbb{E}[f^o(\mathbf{x}_*) y_i^e] &= \beta^{eo} k(\mathbf{x}_i^e, \mathbf{x}_*) \end{aligned}$$

We now write this in vector form. Let us define

$$\mathbf{y} = \begin{bmatrix} \mathbf{y}^e \\ \mathbf{y}^o \end{bmatrix}$$

which is of length  $n_e + n_o$ . We can similarly define  $X = (X^e, X^o)$  which is a  $(n_e + n_o) \times p$  matrix. We then write

$$\mathbf{y} \sim \mathcal{N}(\mathbf{0}, K(X, X) + \sigma^2 I)$$

where

$$K(X, X) = \begin{bmatrix} \beta^e K(X^e, X^e) & \beta^{eo} K(X^e, X^o) \\ \beta^{eo} K(X^o, X^e) & \beta^o K(X^o, X^o) \end{bmatrix}$$

If we similarly write  $\mathbf{f}(\mathbf{x}_*) = (f^e(\mathbf{x}_*), f^o(\mathbf{x}_*))$ , then we have

$$\begin{bmatrix} \mathbf{y} \\ \mathbf{f}(\mathbf{x}_*) \end{bmatrix} \sim \mathcal{N}\left(\mathbf{0}, \begin{bmatrix} K(X, X) + \sigma^2 I & K(X, \mathbf{x}_*) \\ K(\mathbf{x}_*, X) & K(\mathbf{x}_*, \mathbf{x}_*) \end{bmatrix}\right)$$

where

$$\begin{aligned} K(\mathbf{x}_*, \mathbf{x}_*) &= B \otimes k(\mathbf{x}_*, \mathbf{x}_*) \\ K(X, \mathbf{x}_*) &= \begin{bmatrix} \beta^e k(\mathbf{x}_*, X^e) & \beta^{eo} k(\mathbf{x}_*, X^o) \\ \beta^{eo} k(\mathbf{x}_*, X^e) & \beta^o k(\mathbf{x}_*, X^o) \end{bmatrix} \end{aligned}$$

To clarify,  $K(X, \mathbf{x}_*)$  is a  $(n^o + n^e) \times 2$  matrix.

One can then use the usual conditional of a Gaussian distribution, which shows that

$$\mathbf{f}(\mathbf{x}_*) \mid X, \mathbf{y} \sim \mathcal{N}(m_{\mathcal{D}}(\mathbf{x}_*), K_{\mathcal{D}}(\mathbf{x}_*, \mathbf{x}_*))$$

where

$$K_{\mathcal{D}}(\mathbf{x}_*, \mathbf{x}_*) = K(\mathbf{x}_*, \mathbf{x}_*) - K(\mathbf{x}_*, X) [K(X, X) + \sigma^2 I]^{-1} K(X, \mathbf{x}_*).$$

The posterior mean can similarly be defined as

$$\mathbf{m}_{\mathcal{D}}(\mathbf{x}_*) = K(\mathbf{x}_*, X) [K(X, X) + \sigma^2 I]^{-1} \mathbf{y}.$$

## Appendix D. Interpreting $\rho$

For further intuition,  $\rho$  can be interpreted as a measure of codependence between  $f^e$  and  $f^o$ , as formalised by the following result.

**Proposition 2** *We have  $\rho = 1$  if and only if*

$$\alpha_1^e \alpha_2^o = \alpha_1^o \alpha_2^e$$

**Proof** It is easier to work with  $1 - \rho^2$ , where plugging in the values from (Equation 1) gives

$$1 - \rho^2 = \frac{\beta^e \beta^o - (\beta^{eo})^2}{\beta^e \beta^o} = \frac{(\alpha_1^e \alpha_2^o - \alpha_1^o \alpha_2^e)^2}{\beta^e \beta^o}$$

The denominator is positive and finite, so the numerator is thus 0 if and only if  $\alpha_1^e \alpha_2^o = \alpha_1^o \alpha_2^e$ . ■

Assuming non-zero coefficients, this is equivalent to the condition  $\alpha_1^e / \alpha_1^o = \alpha_2^e / \alpha_2^o$ , which implies that  $f^e$  is a scalar multiple of  $f^o$ . It is thus intuitive that this results in  $\rho = 1$ , as learning about  $f^o$  is equivalent to learning about  $f^e$ . Finally, another useful observation is that if a single coefficient is 0, we will have  $\rho < 1$  as long as all other coefficients are non-zero.

## Appendix E. Proof of Proposition 3.1

Consider first updating the GP with the experimental data points. This gives us

$$\mathbf{f}(\mathbf{x}_*) \mid X^e, \mathbf{y}^e \sim \mathcal{N}(m_{\mathcal{D}_e}(\mathbf{x}_*), K_{\mathcal{D}_e}(\mathbf{x}_*, \mathbf{x}_*))$$

where

$$K_{\mathcal{D}_e}(\mathbf{x}_*, \mathbf{x}_*) = K(\mathbf{x}_*, \mathbf{x}_*) - [\beta^e k(\mathbf{x}_*, X^e) \quad \beta^{eo} k(\mathbf{x}_*, X^e)]^T \Sigma_e^{-1} [\beta^e k(\mathbf{x}_*, X^e) \quad \beta^{eo} k(\mathbf{x}_*, X^e)]$$

where

$$\Sigma_e = \beta^e K(X^e, X^e) + \sigma^2 I$$

and  $K(\mathbf{x}_*, \mathbf{x}_*) = B \otimes k(\mathbf{x}_*, \mathbf{x}_*)$ . Note that  $[\beta^e k(\mathbf{x}_*, X^e) \quad \beta^{eo} k(\mathbf{x}_*, X^e)]$  is a  $n^e \times 2$  matrix. The posterior mean can similarly be defined, but is not our focus here.

We can now simply treat  $m_{\mathcal{D}_e}$  and  $K_{\mathcal{D}_e}$  as our prior mean and covariance functions respectively, noting that the covariance function can also be written as

$$K_{\mathcal{D}_e}(\mathbf{x}_*, \mathbf{x}_*) = B \otimes k(\mathbf{x}_*, \mathbf{x}_*) - B' \otimes k'(\mathbf{x}_*, \mathbf{x}_*),$$

where

$$B' = \begin{bmatrix} (\beta^e)^2 & \beta^e \beta^{eo} \\ \beta^e \beta^{eo} & (\beta^{eo})^2 \end{bmatrix}, \quad k'(\mathbf{x}_*, \mathbf{x}_*) = k(\mathbf{x}_*, X^e)^T \Sigma_e^{-1} k(\mathbf{x}_*, X^e)$$

As in the main paper, let us assume that

$$\begin{bmatrix} \alpha_1^e & \alpha_2^e \\ \alpha_1^o & \alpha_2^o \end{bmatrix} = \begin{bmatrix} 1 & 0 \\ \rho & \sqrt{1-\rho^2} \end{bmatrix},$$

which gives

$$B = \begin{bmatrix} 1 & \rho \\ \rho & 1 \end{bmatrix}, \quad B' = \begin{bmatrix} 1 & \rho \\ \rho & \rho^2 \end{bmatrix}.$$

If we now observe  $(X^o, \mathbf{y}^o)$ , then we can write the full posterior as

$$\mathbf{f}(\mathbf{x}_*) \mid X^e, \mathbf{y}^e, X^o, \mathbf{y}^o \sim \mathcal{N}(m_{\mathcal{D}}(\mathbf{x}_*), K_{\mathcal{D}}(\mathbf{x}_*, \mathbf{x}_*)).$$

where the key is that

$$K_{\mathcal{D}}(\mathbf{x}_*, \mathbf{x}_*) = K_{\mathcal{D}_e}(\mathbf{x}_*, \mathbf{x}_*) - K_{\mathcal{D}_e}^o(\mathbf{x}_*, X^o) [K_{\mathcal{D}_e}^o(X^o, X^o) + \sigma^2 I]^{-1} K_{\mathcal{D}_e}^o(X^o, \mathbf{x}_*)$$

where

$$\begin{aligned} K_{\mathcal{D}_e}^o(X^o, X^o) &= \beta^o K(X^o, X^o) - (\beta^{eo})^2 K'(X^o, X^o) \\ &= K(X^o, X^o) - \rho^2 K'(X^o, X^o) \end{aligned}$$

and

$$\begin{aligned} K_{\mathcal{D}_e}^{\circ}(X^{\circ}, \mathbf{x}^*) &= [\beta^{\text{eo}}k(\mathbf{x}^*, X^{\circ}) - \beta^e\beta^{\text{eo}}k'(\mathbf{x}^*, X^{\circ}), \quad \beta^{\circ}k(\mathbf{x}^*, X^{\circ}) - (\beta^{\text{eo}})^2k'(\mathbf{x}^*, X^{\circ})] \\ &= [\rho(k(\mathbf{x}^*, X^{\circ}) - k'(\mathbf{x}^*, X^{\circ})), \quad k(\mathbf{x}^*, X^{\circ}) - \rho^2k'(\mathbf{x}^*, X^{\circ})] \end{aligned}$$

where  $K_{\mathcal{D}_e}^{\circ}(X^{\circ}, \mathbf{x}^*)$  is a matrix of shape  $n^{\circ} \times 2$  and  $K_{\mathcal{D}_e}^{\circ}(\mathbf{x}^*, X^{\circ}) = K_{\mathcal{D}_e}^{\circ}(X^{\circ}, \mathbf{x}^*)^T$ .

We thus have the posterior variance of  $f^e$  as

$$\begin{aligned} V^e(\mathbf{x}_*) &= (k(\mathbf{x}_*, \mathbf{x}_*) - k'(\mathbf{x}_*, \mathbf{x}_*)) \\ &\quad - \rho^2 (k(\mathbf{x}^*, X^{\circ}) - k'(\mathbf{x}^*, X^{\circ}))^T \Sigma_{\text{eo}}^{-1} (k(\mathbf{x}^*, X^{\circ}) - k'(\mathbf{x}^*, X^{\circ})) \end{aligned}$$

where

$$\begin{aligned} \Sigma_{\text{eo}} &= K_{\mathcal{D}_e}^{\circ}(X^{\circ}, X^{\circ}) + \sigma^2 I \\ &= K(X^{\circ}, X^{\circ}) - \rho^2 K'(X^{\circ}, X^{\circ}) + \sigma^2 I. \end{aligned}$$

The first term is the original posterior covariance given  $(X^e, \mathbf{y}^e)$ , whilst the second term is the reduction in variance due to  $\mathcal{D}_o = (X^{\circ}, \mathbf{y}^{\circ})$ , which we want to control. In other words, we want to upper bound

$$\rho^2 (k(\mathbf{x}^*, X^{\circ}) - k'(\mathbf{x}^*, X^{\circ}))^T \Sigma_{\text{eo}}^{-1} (k(\mathbf{x}^*, X^{\circ}) - k'(\mathbf{x}^*, X^{\circ}))$$

We now want to write the above term as the posterior variance of a GP. We can guess the following solution and write:

$$V^e(\mathbf{x}_*) = (1 - \rho^2) (k(\mathbf{x}_*, \mathbf{x}_*) - k'(\mathbf{x}_*, \mathbf{x}_*)) + \rho^2 P$$

where

$$\begin{aligned} P &= (k(\mathbf{x}_*, \mathbf{x}_*) - k'(\mathbf{x}_*, \mathbf{x}_*)) \\ &\quad - (k(\mathbf{x}^*, X^{\circ}) - k'(\mathbf{x}^*, X^{\circ}))^T \Sigma_{\text{eo}}^{-1} (k(\mathbf{x}^*, X^{\circ}) - k'(\mathbf{x}^*, X^{\circ})). \end{aligned}$$

If we can show that  $P \geq 0$ , then we are done. To see this, note that we can apply Woodbury's matrix identity which gives

$$\begin{aligned} \Sigma_{\text{eo}}^{-1} &= [ \underbrace{(1 - \rho^2)K'(X^{\circ}, X^{\circ})}_A + \underbrace{K(X^{\circ}, X^{\circ}) - K'(X^{\circ}, X^{\circ}) + \sigma^2 I}_B ]^{-1} \\ &= B^{-1} - \underbrace{(B + BA^{-1}B)^{-1}}_C \end{aligned}$$

which gives

$$\begin{aligned} P &= (k(\mathbf{x}_*, \mathbf{x}_*) - k'(\mathbf{x}_*, \mathbf{x}_*)) - (k(\mathbf{x}^*, X^{\circ}) - k'(\mathbf{x}^*, X^{\circ}))^T B^{-1} (k(\mathbf{x}^*, X^{\circ}) - k'(\mathbf{x}^*, X^{\circ})) \\ &\quad + \underbrace{(k(\mathbf{x}^*, X^{\circ}) - k'(\mathbf{x}^*, X^{\circ}))^T C (k(\mathbf{x}^*, X^{\circ}) - k'(\mathbf{x}^*, X^{\circ}))}_{\geq 0} \end{aligned}$$

To show the final term is positive, we just need to show that  $C$  is positive semi-definite which implies  $x^T C x \geq 0$  for any vectors  $x$ . If  $A$  and  $B$  are positive definite (PD) and symmetric, then so is  $A^{-1}$  and  $BA^{-1}B$ . The sum of two PD matrices is PD, as is the inverse of a PD matrix, so  $C$  is PD. Finally, we see that the remaining first terms in  $P$  is simply the regular posterior variance (given  $\mathcal{D}_o$ ) of a GP with kernel  $k(\mathbf{x}_*, \mathbf{x}_*) - k'(\mathbf{x}_*, \mathbf{x}_*)$ , which is non-negative.

Putting this together then, we have

$$V^e(\mathbf{x}_*) \geq (1 - \rho^2) V_{\mathcal{D}_e}^e(\mathbf{x}_*)$$

where  $V_{\mathcal{D}_e}^e$  is the variance conditional on  $\mathcal{D}_e = (X^e, \mathbf{y}^e)$  only.

## Appendix F. Confounding function

The hidden confounding function  $\eta(\mathbf{x}) = f^e(\mathbf{x}) - f^o(\mathbf{x})$  quantifies the degree to which conditional average treatment effect in the observational study deviates from the conditional average treatment effect in the trial. This may be of independent interest in order to understand the underlying process for treatment assignment or allocation in the real-world outside of the experimental setting. Although our principal focus in the above exposition is on  $f^e$ , we may also easily obtain a posterior distribution for  $\eta(\mathbf{x})$ , by considering the joint posterior distribution over  $\mathbf{f}(\mathbf{x})$ .

### F.1. Variance of confounding function

Suppose we now want to compute the variance of the confounding function evaluated at  $\mathbf{x}_*$ . This is given by  $\eta(\mathbf{x}_*) = f^e(\mathbf{x}_*) - f^o(\mathbf{x}_*)$ , or in matrix notation  $\eta(\mathbf{x}_*) = \begin{pmatrix} 1 \\ -1 \end{pmatrix}^T \mathbf{f}(\mathbf{x}_*)$ . By standard properties of the multivariate Gaussian distribution, it follows that

$$\eta(\mathbf{x}_*) \mid X, \mathbf{y} \sim \mathcal{N}(m^e(\mathbf{x}_*) - m^o(\mathbf{x}_*), V_\eta(\mathbf{x}_*)),$$

where

$$\begin{aligned} V_\eta(\mathbf{x}_*) &= \begin{pmatrix} 1 \\ -1 \end{pmatrix}^T K_*(\mathbf{x}_*, \mathbf{x}_*) \begin{pmatrix} 1 \\ -1 \end{pmatrix} \\ &= (\beta^e + \beta^o - 2\beta^{eo})k(\mathbf{x}_*, \mathbf{x}_*) \\ &\quad - \begin{pmatrix} (\beta^e - \beta^{eo})k(\mathbf{x}_*, X^e) \\ (\beta^{eo} - \beta^o)k(\mathbf{x}_*, X^o) \end{pmatrix}^T [K(X, X) + \sigma^2 I]^{-1} \begin{pmatrix} (\beta^e - \beta^{eo})k(\mathbf{x}_*, X^e) \\ (\beta^{eo} - \beta^o)k(\mathbf{x}_*, X^o) \end{pmatrix} \\ &= 2(1 - \rho)k(\mathbf{x}_*, X^e) - \begin{pmatrix} (1 - \rho)k(\mathbf{x}_*, X^e) \\ (\rho - 1)k(\mathbf{x}_*, X^o) \end{pmatrix}^T [K(X, X) + \sigma^2 I]^{-1} \begin{pmatrix} (1 - \rho)k(\mathbf{x}_*, X^e) \\ (\rho - 1)k(\mathbf{x}_*, X^o) \end{pmatrix} \end{aligned}$$

## Appendix G. Multivariate simulation studies

### G.1. Multivariate Data Generation Process

Similar to the univariate case, in the multivariate case we vary the complexity of the confounding and the CATE function, but we choose to explore only cases with nonlinear potential outcomes functions.

Simulation 1: Nonlinear Potential Outcomes, linear confounding, linear CATE

Assume that we have five continuous baseline covariate  $X_j \sim U[-2, 2]$ , where  $j = 1, \dots, 5$ . The values of  $X$  define the trial participation mechanism defined as  $S \sim \text{Bernoulli}(p_S)$  where  $p_S = \frac{\exp(-10-8X_1-8X_2)}{1+\exp(-10-8X_1-8X_2)}$ . After selecting all trial participants we assign them randomly to treatment  $A \sim \text{Bernoulli}(0.5)$ . The potential outcomes are generated as  $Y(a) = a\tau(X) + \sum_{j=1}^5 X_j + \epsilon$ , for  $a = 0, 1$ , where  $\tau(X) = 1 + X_1 + X_2$  is the CATE and  $\epsilon \sim \mathcal{N}(0, 1)$ . For the observational study we have  $X_j \sim U[-2, 2]$ , where  $j = 1, \dots, 5$ , and the treatment is generated according to the model  $A \sim \text{Bernoulli}(e(X))$  where  $\text{logit}(e(X)) = -(X_1 + X_2)$ . Similarly to the trial the potential outcomes are  $Y(a) = a\tau(X) + \sum_{j=1}^5 X_j + U + \epsilon$ , for  $a = 0, 1$ .  $U$  represents the hidden confounding and we generated as  $U \sim \mathcal{N}((2A - 1)(X_1 + X_2), 1)$ .

Simulation 2: Nonlinear Potential Outcomes, nonlinear confounding, nonlinear CATE

Assume that we have five continuous baseline covariate  $X_j \sim U[-2, 2]$ , where  $j = 1, \dots, 5$ . The values of  $X$  define the trial participation mechanism defined as  $S \sim \text{Bernoulli}(p_S)$  where  $p_S = \frac{\exp(-10-8X_1-8X_2)}{1+\exp(-10-8X_1-8X_2)}$ . After selecting all trial participants we assign them randomly to treatment  $A \sim \text{Bernoulli}(0.5)$ . The potential outcomes are generated as  $Y(a) = a\tau(X) + \sum_{j=1}^5 X_j + \epsilon$ , for  $a = 0, 1$ , where  $\tau(X) = 1 + X_1 + X_1^2 + X_2 + X_2^2$  is the CATE and  $\epsilon \sim \mathcal{N}(0, 1)$ . For the observational study we have  $X_j \sim U[-2, 2]$ , where  $j = 1, \dots, 5$ , and the treatment is generated according to the model  $A \sim \text{Bernoulli}(e(X))$  where  $\text{logit}(e(X)) = -(X_1 + X_2)$ . Similarly to the trial the potential outcomes are  $Y(a) = a\tau(X) + \sum_{j=1}^5 X_j + U + \epsilon$ , for  $a = 0, 1$ .  $U$  represents the hidden confounding and we generated as  $U \sim \mathcal{N}((2A - 1)(\sin(X_1) + \sin(X_2)), 1)$ .

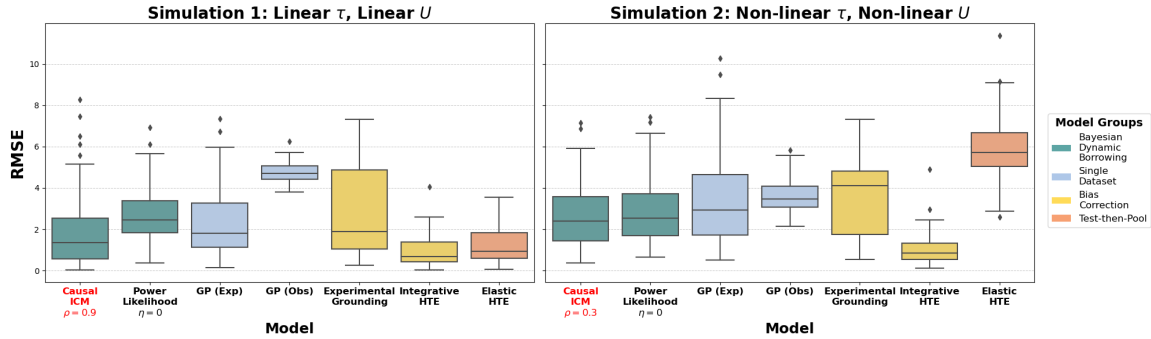


Figure 4: Multivariate simulation results over 100 simulated datasets. *Left*: Simulation setting 1: linear CATE and unobserved confounding, *Right*: Non-linear CATE and unobserved confounding

**G.2. Multivariate Simulations: Results**

Based on Figure 4, in the first simulation setting, the highest performance is achieved by the Integrative HTE and the Elastic HTE, as expected given that both models are correctly specified. Notably, the performance of *Causal-ICM* is comparable to these benchmarks, demonstrating its competitiveness even when the models are well-specified.

In the second simulation setting, where both the [CATE](#) and the confounding exhibit more complex, non-linear structures, the performance of models relying on correct specification deteriorates. In contrast, *Causal-ICM* maintains robust performance, being outperformed only by the Integrative HTE. Importantly, this superior performance of the Integrative HTE is a consequence of having a correctly specified outcome model; in realistic scenarios where model specification is uncertain or misspecified, we expect *Causal-ICM* to offer more reliable and consistent results.

## Appendix H. Extrapolation with *Causal-ICM*

Below we show the performance of *Causal-ICM* in the first univariate simulation setting, where both the [CATE](#) and the confounding functions are non-linear. The *Causal-ICM* can successfully produce accurate estimates of the [CATE](#) both within and outside the support of the [RCT](#) with inflated uncertainty outside the support.

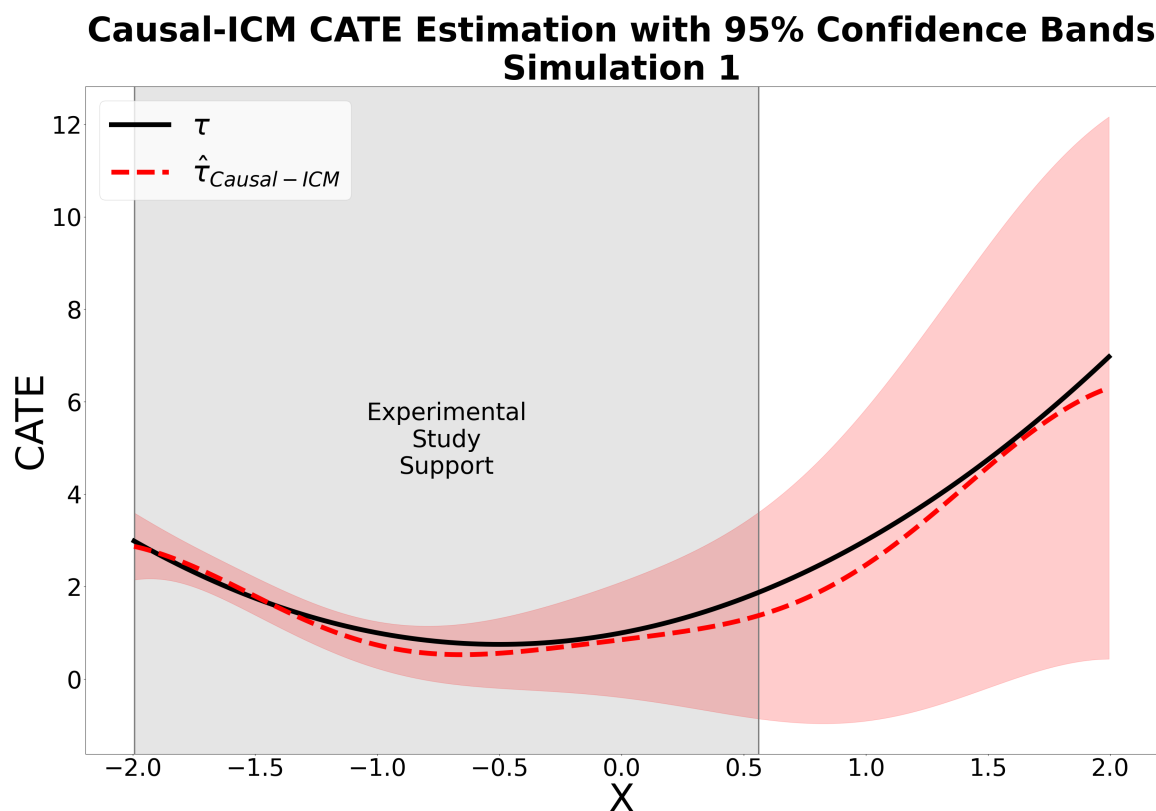


Figure 5: Estimated CATE under the first univariate simulation setting with nonlinear CATE and confounding functions.

## Appendix I. Sensitivity to the parameter $\rho$ , the sample size of the observational study, the kernel choice and the degree of overlap

Below we present a more thorough exploration of the effects of different values of  $\rho$ , differing observational/experimental sample sizes, the choice of kernel and the degree of overlap between the two studies for the second simulation setting of the main text where the [CATE](#) and the confounding function are non-linear.

$\rho$	RMSE
0.0	2.571
0.2	2.051
0.4	1.502
0.6	0.913
0.8	0.305
1.0	1.095

Table 2: RMSE values for different values of  $\rho$ , Univariate simulation 2

Kernel	Mean RMSE (SD)
RBF	0.822 (0.651)
Matérn 3/2	1.315 (0.0556)
Matérn 5/2	0.968 (0.583)

Table 3: Mean RMSE for different kernels, Univariate simulation 2

Sample size	Mean RMSE (SD)
$n^{(e)} = 100, n^{(0)} = 100$	0.879 (0.484)
$n^{(e)} = 100, n^{(0)} = 500$	0.797 (0.524)
$n^{(e)} = 100, n^{(0)} = 1000$	0.731 (0.448)
$n^{(e)} = 100, n^{(0)} = 2000$	0.793 (0.481)

Table 4: Mean RMSE for different sample sizes, Univariate simulation 2; Results obtained over 50 different simulated datasets.

The results above show that

1.  $\rho$  indeed plays an important role in controlling the influence of the unobserved confounding
2. *Causal-ICM* retains strong performance for different kernels, or even as the sample size of the (confounded) observational data grows
3. The *Causal-ICM* performs well even with low overlap between the two studies, although optimal results are obtained with full overlap.

Overlap	Optimal $\rho$	Mean RMSE (SD)
Full	0.5	0.264 (0.088)
High	0.4	0.444 (0.237)
Low	0.8	0.941 (0.607)

Table 5: Mean RMSE for different degrees of overlap between the [RCT](#) and observational study for the second simulation setting of the main text (Univariate simulation 2); The degree of overlap is controlled through the coefficients of the model for study participation; Results obtained over 100 different simulated datasets.

## Appendix J. Priors for latent processes, extensions to non-Gaussian likelihoods, and computational complexity

In the current implementation of *Causal-ICM*, both  $u_1(x)$  and  $u_2(x)$  share the same kernel hyperparameters (lengthscale, variance). However, extensions to the model do exist that allow  $u_1(x)$  and  $u_2(x)$  to originate from distinct Gaussian Processes, such as in the Linear Model of Coregionalization (LCM) [Alvarez et al. \(2012\)](#). Exploring these extensions represents a promising direction for future research.

With respect to extensions to non-Gaussian likelihoods, our theoretical results currently rely on the conjugacy of the Gaussian likelihood, which greatly simplifies the proofs. Nevertheless, we anticipate that similar results can be extended to other likelihoods that have closed-form posterior variances, such as the Student-T process. We expect these extensions to be non-trivial, however, and so leave these for future work.

For likelihoods requiring approximation methods, such as the Bernoulli likelihood, the analysis becomes significantly more intricate compared to conjugate cases. Nevertheless, we are actively exploring this direction as part of our efforts to extend causal-ICM to accommodate binary outcomes. A promising avenue involves employing a sigmoid link function to transform Gaussian Process outputs into the  $[0,1]$  interval, enabling compatibility with binary targets. While we expect comparable results in this setting, posterior approximations will be necessary. This extension represents a significant focus of our ongoing research and will play a central role in our future developments.

Last, [GPs](#) are known for their computational complexity. In our examples, we utilize the full GP as the datasets are not too large. However, their cubic computational scaling with the number of data points is indeed a well-recognized limitation when datasets are larger. To mitigate this issue, we suggest using sparse GPs as an approximation method, where we reduce computational cost by relying on a subset of the data (i.e. inducing points) to approximate the full GP model.